# **NOTE:**

This preprint has not undergone peer review or any post-submission improvements or corrections. The Version of Record of this contribution is published in "Emerging Technologies in Computational Sciences for Industry, Sustainability and Innovation", and is available online at https://doi.org/10.1007/978-3-031-95709-3\_18.

# A Discontinuous Galerkin Discretization for the Intrinsic Beam Model

Christian Bleffert<sup>[0009-0004-1957-292X]</sup>, Lukas Dreyer<sup>[0000-0001-7484-3674]</sup> and Melven Röhrig-Zöllner<sup>[0000-0001-9851-5886]</sup>

## 1 Introduction

In this chapter, we are concerned with the *Geometrically Exact, Intrinsic Model for Dynamics of Curved and Twisted Anisotropic Beams*. The model was developed in 2003 by Hodges [1]. In the following, we refer to it as *Intrinsic Beam* (IB) model. As a geometrically exact formulation, it allows to model beams undergoing large deformations, making it particularly interesting for applications regarding highly flexible structures such as helicopter blades [2, 3].

We are interested in using the model to simulate the rotor blades of rotary-wing aircraft. Therefore, we focus on beams that are clamped at one end (rotor head) and free swinging at the other (blade tip).

The intrinsic beam equations are a system of partial differential equations (PDEs) in one spatial dimension and in time. We formulate the equations as a system of linear hyperbolic balance laws. A similar formulation is derived in [4], where it is also shown that the underlying system is indeed hyperbolic. We then discretize the equations in space using a *Discontinuous Galerkin* (DG) method as commonly used for hyperbolic balance laws, see, e.g., [5, 6, 7, 8].

Christian Bleffert

Deutsches Zentrum für Luft- und Raumfahrt e.V., Linder Höhe, 51147 Cologne, Germany, e-mail: christian.bleffert@dlr.de

Lukas Dreyer

Deutsches Zentrum für Luft- und Raumfahrt e.V., Lilienthalplatz 7, 38108 Braunschweig, Germany, e-mail: lukas.dreyer@dlr.de

Melven Röhrig-Zöllner

Deutsches Zentrum für Luft- und Raumfahrt e.V., Linder Höhe, 51147 Cologne, Germany, e-mail: melven.roehrig-zoellner@dlr.de

## 2 The Intrinsic Beam Model

In this section, we consider theoretical aspects. We first introduce the governing equations in the form they were originally derived in [1]. Based on this, we present and analyse the formulation as linear hyperbolic balance law from [4].

## 2.1 Original Formulation of the Equations

We start with some preliminary definitions required for the IB equations. For more details, see [1, 9].

We consider a beam that is, in general, initially curved and twisted and of anisotropic material. We describe the geometry of the beam by a one-dimensional reference line (also called centerline) of initial length  $\ell$  which is the elastic axis of the beam. The beam is clamped at one end (x=0) and free swinging at the other  $(x=\ell)$ , where x is the running length coordinate along the undeformed beam axis. We consider the behavior of the beam in a given time interval [0,T] and use t to denote the time coordinate. All following quantities are 'body-attached', meaning that they are expressed in the coordinate system of the deformed beam (at the reference line).

Let F(x,t) denote the internal forces of the beam, M(x,t) the internal moments, V(x,t) the linear velocities,  $\Omega(x,t)$  the angular velocities, k(x) the initial curvature of the beam,  $\kappa(x,t)$  the angular strains,  $\gamma(x,t)$  the linear strains, P(x,t) the linear momentum, H(x,t) the angular momentum,  $f_{\text{ext}}(x,t)$  external forces acting along the beam and  $m_{\text{ext}}(x,t)$  external moments. All defined quantities in this paragraph have values in  $\mathbb{R}^3$ . Where it is clear from the context, we omit the dependency on (x,t).

To shorten the notation, we write a *cross-product matrix* as:

$$\tilde{w} := \begin{pmatrix} 0 & -w_3 & w_2 \\ w_3 & 0 & -w_1 \\ -w_2 & w_1 & 0 \end{pmatrix}, \quad \text{for } w := \begin{pmatrix} w_1 \\ w_2 \\ w_3 \end{pmatrix} \in \mathbb{R}^3.$$

So,  $\tilde{w}z = w \times z$  for  $w, z \in \mathbb{R}^3$ . Let finally  $e_1 := (1, 0, 0)^T$ .

The intrinsic beam model can now be formulated as

$$F' + (\tilde{k} + \tilde{\kappa})F + f_{\text{ext}} = \dot{P} + \tilde{\Omega}P ,$$

$$M' + (\tilde{k} + \tilde{\kappa})M + (\tilde{e_1} + \tilde{\gamma})F + m_{\text{ext}} = \dot{H} + \tilde{\Omega}H + \tilde{V}P ,$$

$$V' + (\tilde{k} + \tilde{\kappa})V + (\tilde{e_1} + \tilde{\gamma})\Omega = \dot{\gamma} ,$$

$$\Omega' + (\tilde{k} + \tilde{\kappa})\Omega = \dot{\kappa} ,$$

$$(1)$$

for  $x \in (0, \ell)$  and  $t \in (0, T)$ , where  $(\cdot)'$  denotes the partial derivative with respect to x and  $(\cdot)$  denotes the partial derivative with respect to t.

#### 2.2 Constitutive Laws

The system (1) contains 8 unknown vectors  $(F, M, V, \Omega, \kappa, \gamma, P, H)$  but provides only 4 vector equations. To close the formulation, we employ two *constitutive laws*: The *mass matrix*  $M(x) \in \mathbb{R}^{6\times 6}$  relates the linear and angular momentum vectors P, H to the linear and angular velocity vectors  $V, \Omega$ . The *flexibility matrix*  $C(x) \in \mathbb{R}^{6\times 6}$  relates the linear and angular strains  $\gamma, \kappa$  to the internal forces and moments F, M. Together, this results in the following constitutive equations as also used for example in [1, 9, 10]:

$$\begin{pmatrix} P \\ H \end{pmatrix} = \mathcal{M} \begin{pmatrix} V \\ \Omega \end{pmatrix} , \qquad \begin{pmatrix} \gamma \\ \kappa \end{pmatrix} = C \begin{pmatrix} F \\ M \end{pmatrix} . \qquad (2)$$

Specific values of  $\mathcal{M}$  and  $\mathcal{C}$  depend on the material properties of the modeled beam and are not relevant for the purpose of this paper. Both  $\mathcal{M}$  and  $\mathcal{C}$  are symmetric and assumed to be positive definite. For more details, see [1, 9]. This allows to combine both constitutive laws into one equation using:

$$\begin{pmatrix} P \\ H \\ \gamma \\ \kappa \end{pmatrix} = -A^{-1} \begin{pmatrix} F \\ M \\ V \\ \Omega \end{pmatrix} \qquad \text{with } A := -\begin{pmatrix} 0 & \mathcal{M} \\ C & 0 \end{pmatrix}^{-1} . \tag{3}$$

## 2.3 Formulation as Linear Hyperbolic Balance Law

By writing the system (1) in a matrix-vector form and plugging in (3), we can obtain a linear balance law. For this type of PDE system, there exists extensive literature, especially regarding its discretization with DG methods such as [5, 6, 8]. This literature provides the basis for our analysis.

More precisely, using  $u(x,t) := (F^T, M^T, V^T, \Omega^T)^T \in \mathbb{R}^{12}$ , the intrinsic beam equations result in the following *advective form* of a linear balance law:

$$u_t + Au_x = Q_{\text{adv}}(u) , \qquad (4)$$

where we now use  $(\cdot)_x$  and  $(\cdot)_t$  as a notation for the partial derivatives with respect to x and t, respectively, to facilitate the notation in terms of the discretization in Sect. 3. The source term  $Q_{\text{adv}}$  is given by:

$$Q_{\text{adv}}(u) := -A \left( \begin{pmatrix} E & 0 \\ 0 & -E^T \end{pmatrix} + \begin{pmatrix} \mathcal{L}(Cs) & 0 \\ 0 & -\mathcal{L}^T(Cs) \end{pmatrix} - \begin{pmatrix} 0 & \mathcal{L}(y)\mathcal{M} \\ 0 & 0 \end{pmatrix} \right) u - A\hat{q}_{\text{ext}}$$
 (5)

with 
$$s := (u_1, \dots, u_6)$$
,  $y := (u_7, \dots, u_{12})$ ,  $\hat{q}_{\text{ext}} = (f_{\text{ext}}^T, m_{\text{ext}}^T, 0, 0)^T$ , the matrix

$$E(x) := \begin{pmatrix} \tilde{k} & 0 \\ \tilde{e_1} & \tilde{k} \end{pmatrix} ,$$

and the linear operator  $\mathcal{L}: \mathbb{R}^6 \to \mathbb{R}^{6 \times 6}$  defined as

$$\mathcal{L}(z) := \begin{pmatrix} \tilde{z_2} & 0 \\ \tilde{z_1} & \tilde{z_2} \end{pmatrix}, \quad \text{with } z_1, z_2 \in \mathbb{R}^3, \ z := \begin{pmatrix} z_1 \\ z_2 \end{pmatrix}.$$

This useful notation for  $\mathcal{L}$  is adopted from [11]. From the definition of the source term, we see that the balance law contains non-linearities of degree two that result from the multiplication of the second and third matrix in (5) with u.

If we multiply the advective form of the balance law (4) with the block-diagonal matrix  $\Gamma$  of the flexibility and mass matrices, we obtain the following *capacity form* of the equation:

$$\Gamma u_t + \Pi u_x = Q(u) . ag{6}$$

Here, the matrices  $\Gamma(x)$  and  $\Pi$  are defined as:

$$\Gamma(x) := \begin{pmatrix} C & 0 \\ 0 & \mathcal{M} \end{pmatrix}, \qquad \Pi := -\begin{pmatrix} 0 & I \\ I & 0 \end{pmatrix} \;,$$

where I denotes the  $6 \times 6$  identity matrix. The source term Q is then:

$$Q(u) := \Gamma Q_{\text{adv}}(u) = \left( \begin{pmatrix} 0 & -E^T \\ E & 0 \end{pmatrix} + \begin{pmatrix} 0 & -\mathcal{L}^T(Cs) \\ \mathcal{L}(Cs) & 0 \end{pmatrix} - \begin{pmatrix} 0 & 0 \\ 0 & \mathcal{L}(y)\mathcal{M} \end{pmatrix} \right) u + q_{\text{ext}} ,$$
(7)

where  $q_{\text{ext}} := (0, 0, f_{\text{ext}}^T, m_{\text{ext}}^T)^T$ .

Note that Eqs. (4) and (6) are in fact equivalent. The latter one, however, enables *summation-by-parts* of the discrete operator, which facilitates the energy analysis of the solution in the discrete context as we will see in Sect. 3.

In [4], an explicit form of the transformation matrix T is constructed that diagonalizes the system matrix A. For the scope of this chapter, we do not need the full definition of T and refer the reader to [4]. More details about the following derivations can be found in [12]. However, the matrix T has a specific block structure that allows us to derive mathematically useful boundary conditions. More precisely, T consists of two invertible matrices  $T_1(x), T_2(x) \in \mathbb{R}^{6 \times 6}$  with:

$$T = \frac{1}{2} \begin{pmatrix} T_1 & T_1 \\ T_2 & -T_2 \end{pmatrix} \; , \qquad \qquad T^{-1} = \begin{pmatrix} T_1^{-1} & T_2^{-1} \\ T_1^{-1} & -T_2^{-1} \end{pmatrix} \; .$$

Through this, we obtain the following expression for the eigenvalues of A (see [12]):

$$\Lambda = T^{-1}AT$$
 with  $\Lambda = \begin{pmatrix} -\Lambda & 0 \\ 0 & \Lambda \end{pmatrix}$ ,

where  $\Lambda = \Lambda(x)$  is a real, positive  $6 \times 6$  diagonal matrix which shows that the balance law is hyperbolic.

With the transformation matrix T we can transform the system into *characteristic* variables  $w(x,t) := T^{-1}(x)u(x,t)$  resulting in the following equivalent balance law with a diagonal advection matrix:

$$w_t + \Lambda w_x = Q_{\text{char}}(w)$$
, with  $Q_{\text{char}}(w) = T^{-1}Q_{\text{adv}}(Tw)$ . (8)

This form is especially helpful for deriving boundary conditions as  $\Lambda$  contains the characteristic speeds at which information propagates through the domain.

## 2.4 Boundary Conditions

To derive the right boundary conditions, on the one hand we have to have the mechanical setup of interest in mind, which is a clamped-free beam. For this setup, we need to prescribe velocities at the clamped end,  $y(0,t) = y_0(t)$ , and internal forces and moments at the free end,  $s(\ell,t) = s_{\ell}(t)$  [13]. On the other hand, not all boundary conditions necessarily lead to a mathematically well-posed problem.

For characteristic variables associated with negative values on the diagonal of  $\Lambda$ , boundary conditions have to be specified at the right boundary. Contrary, characteristic variables associated with positive values of  $\Lambda$  have to have boundary conditions at the left boundary. From the previous section, we know that  $\Lambda$  has a specific structure with the first six diagonal entries being negative and the last six ones being positive. In the following, we will denote the characteristic variables associated with positive entries of  $\Lambda$  as  $w_+$  and the ones associated with negative values as  $w_-$ . Moreover, we will refer to the variables for which we have to provide boundary conditions as *ingoing variables* and to the other ones as *outgoing variables* at the respective boundary.

Guided by [14, 15], we first choose a general class of boundary conditions, allowing the ingoing variables to depend linearly on the outgoing ones and some external data:

$$w_{+}(0,t) = R_{0}w_{-}(0,t) + g_{0}(t) ,$$
  

$$w_{-}(\ell,t) = R_{\ell}w_{+}(\ell,t) + g_{\ell}(t) ,$$
(9)

for external boundary functions  $g_0, g_\ell$  and matrices  $R_0, R_\ell \in \mathbb{R}^{6 \times 6}$ . Again, if misunderstandings are ruled out, we will omit the dependency on t and x.

By definition, the vector of characteristic variables, w, can be written as

$$w = \begin{pmatrix} w_{-} \\ w_{+} \end{pmatrix} = T^{-1}u = \begin{pmatrix} T_{1}^{-1} & T_{2}^{-1} \\ T_{1}^{-1} & -T_{2}^{-1} \end{pmatrix} \begin{pmatrix} s \\ y \end{pmatrix} = \begin{pmatrix} T_{1}^{-1}s + T_{2}^{-1}y \\ T_{1}^{-1}s - T_{2}^{-1}y \end{pmatrix} . \tag{10}$$

Now choosing  $R_0 = I$ , i.e.  $w_+(0, t) = w_-(0, t) + g_0(t)$ , and tracing the above expression back to physical variables yields

$$u|_{x=0} = T \left( \frac{T_1^{-1}s + T_2^{-1}y}{T_1^{-1}s + T_2^{-1}y + g_0} \right) \Big|_{x=0} = \frac{1}{2} \left( \frac{2s + 2T_1T_2^{-1}y + T_1g_0}{-T_2g_0} \right) \Big|_{x=0} . \tag{11}$$

With  $g_0 = -2T_2^{-1}y_0$  the above expression reads

$$u|_{x=0} = \begin{pmatrix} s|_{x=0} \\ y_0 \end{pmatrix} . \tag{12}$$

This means that for this specific choice of  $R_0$  and  $g_0$ , the correct boundary conditions in characteristic variables are equivalent to Dirichlet boundary conditions for the velocities at x = 0. Analogously, choosing  $R_{\ell} = -I$  and  $g_{\ell} = 2T_1^{-1}s_{\ell}$  at the right boundary, we obtain:

$$u|_{x=\ell} = \begin{pmatrix} s_{\ell} \\ y|_{x=\ell} \end{pmatrix} . \tag{13}$$

So for this choice, the correct boundary conditions in characteristic variables are equivalent to Dirichlet boundary conditions for the internal forces and moments at  $x = \ell$ .

Note that by switching the choice of  $R_0$  and  $R_\ell$  and setting  $g_0$  and  $g_\ell$  accordingly, boundary conditions for characteristic variables can also be set in a way that for physical variables we prescribe velocities at  $x = \ell$  and internal forces and moments at x = 0, so that the underlying beam is clamped at  $x = \ell$ .

By choosing an appropriate initial condition  $u_0$ , we can finally formulate the following *initial boundary value problem* (IBVP): Find  $u = (s^T, y^T)^T$ , such that

$$\begin{cases} \Gamma u_{t} + \Pi u_{x} = Q(u) & \text{for } (x,t) \in (0,\ell) \times (0,T) ,\\ y(0,t) = y_{0}(t) & \text{for } t \in (0,T) ,\\ s(\ell,t) = s_{\ell}(t) & \text{for } t \in (0,T) ,\\ u(x,0) = u_{0}(x) & \text{for } x \in [0,\ell] . \end{cases}$$
(14)

## 2.5 Continuous Energy Analysis

Before we actually analyse the solution of the system regarding its energy, we derive a weak formulation of the balance law. Let  $\langle \cdot, \cdot \rangle$  be the inner product in the space of square integrable  $\mathbb{R}^{12}$ -valued functions on  $[0,\ell]$ , i.e.  $\mathbb{L}^2([0,\ell])^{12}$ . Let further  $\|\cdot\|_{\Gamma}$  be the norm induced by the inner product  $\langle \cdot, \cdot \rangle_{\Gamma}$  where  $\langle g, h \rangle_{\Gamma} = \langle g, \Gamma h \rangle$ . We will refer to  $\|g\|_{\Gamma}$  as the *energy norm* of g and to  $\|g\|_{\Gamma}^2$  as the *energy* of g.

The weak formulation of the balance law in capacity form is obtained by multiplying the equation by an appropriate smooth test function  $\varphi$  and integrating over the domain  $[0, \ell]$  which yields

$$\langle \Gamma u_t, \varphi \rangle + \langle \Pi u_x, \varphi \rangle = \langle Q(u), \varphi \rangle$$
 (15)

Integration by parts for the second term of the above left hand side results in

$$\langle \Gamma u_t, \varphi \rangle + (\Pi u)^T \varphi \Big|_{x=0}^{\ell} - \langle \Pi u, \varphi_x \rangle = \langle Q(u), \varphi \rangle .$$
 (16)

For the analysis of the solution's energy we make use of the energy method, similar to [6, 14, 15], and choose  $\varphi = u$  as a test function. Equation (16) then becomes

$$\frac{1}{2}\frac{\mathrm{d}}{\mathrm{d}t}\|u\|_{\Gamma}^{2} + u^{T}\Pi u\Big|_{x=0}^{\ell} - \langle \Pi u, u_{x} \rangle = \langle Q(u), u \rangle . \tag{17}$$

So, there are three terms contributing to the change of the solution's energy. A surface term, a volume term and a term emerging from the source term Q.

Recall the definition of Q from Sect. 2.3:

$$Q(u) = \left( \begin{pmatrix} 0 & -E^T \\ E & 0 \end{pmatrix} + \begin{pmatrix} 0 & -\mathcal{L}^T(Cs) \\ \mathcal{L}(Cs) & 0 \end{pmatrix} - \begin{pmatrix} 0 & 0 \\ 0 & \mathcal{L}(y)\mathcal{M} \end{pmatrix} \right) u + q_{\rm ext} \ .$$

The first two matrices are skew-symmetric, so that the corresponding terms in (17) vanish. The integrand of the term resulting from the third matrix is  $y^T \mathcal{L}(y) \mathcal{M} y$ , which again vanishes as  $y^T \mathcal{L}(y) = 0$  due to the definition of  $\mathcal{L}$ . So, only the contribution of the external sources remains:

$$\langle Q(u), u \rangle = \langle q_{\text{ext}}, u \rangle$$
 (18)

Note, that the vanishing terms vanish point wise and that this is independent of u being a solution of the underlying system. It is a consequence of the special symmetry of the source terms and the linear operator  $\mathcal{L}$ . This important observation will also be used for the discrete energy analysis in Sect. 3.3. The volume term in (17) can be integrated by parts again:

$$\langle \Pi u, u_x \rangle = \frac{1}{2} \left. u^T \Pi u \right|_{x=0}^{\ell} , \qquad (19)$$

as  $\Pi$  is constant and symmetric. Together, this results in the following energy equation:

$$\frac{1}{2} \frac{d}{dt} \|u\|_{\Gamma}^{2} = -\frac{1}{2} u^{T} \Pi u \Big|_{x=0}^{\ell} + \langle q_{\text{ext}}, u \rangle .$$
 (20)

On the one hand, the above equation shows energy conservation in a mathematical sense: The energy of the solution changes only through the boundaries or due to actual external sources. On the other hand, the particular choice of mathematical energy coincides with the total mechanical energy of the modeled beam [1]. The right-hand side of (20) is the sum of work at the boundaries and work due to external forces and moments. So, this reproduces the energy conservation result from [1] but is based on the weak form of the problem.

To show that the IBVP (14) is well-posed, we further need to bound the right-hand side of Eq. (20). We impose the boundary conditions for the surface term using the

representation in characteristic variables and follow the argumentation of [14, 15]. This results in:

$$-\frac{1}{2} \left. u^T \Pi u \right|_{x=0}^\ell = -\frac{1}{2} \left. w^T T^T \Pi T w \right|_{x=0}^\ell = -\frac{1}{4} \left. w^T \Lambda w \right|_{x=0}^\ell \ .$$

For the general boundary conditions defined in Sect. 2.4, we obtain:

$$-\frac{1}{2} u^{T} \Pi u \Big|_{x=0}^{\ell} = \frac{1}{4} \left( \begin{pmatrix} w_{-} \\ g_{0} \end{pmatrix}^{T} \begin{pmatrix} R_{0}^{T} \Lambda R_{0} - \Lambda (\Lambda R_{0})^{T} \\ \Lambda R_{0} & \Lambda \end{pmatrix} \begin{pmatrix} w_{-} \\ g_{0} \end{pmatrix} \Big|_{x=0}$$

$$- \begin{pmatrix} w_{+} \\ g_{\ell} \end{pmatrix}^{T} \begin{pmatrix} -R_{\ell}^{T} \Lambda R_{\ell} + \Lambda - (\Lambda R_{\ell})^{T} \\ -\Lambda R_{\ell} & -\Lambda \end{pmatrix} \begin{pmatrix} w_{+} \\ g_{\ell} \end{pmatrix} \Big|_{x=\ell}$$

$$(21)$$

As shown in [14], these terms are bounded if the matrices  $R_i^T \Lambda R_i - \Lambda$  are negative definite:

$$R_i^T \Lambda R_i - \Lambda < 0,$$
 for  $i = 0, \ell$ . (22)

Unfortunately, for our desired boundary conditions, we have  $R_i = \pm I$  and thus  $R_i^T \Lambda R_i - \Lambda = 0$ . In this case, we cannot apply the approach from [14]. This also has a physical interpretation: the performed work depends on the product of the velocities with forces and moments at the boundary. So, in general, for our choice of boundary condition, the change in mechanical energy depends on the current solution at the boundary for non-zero external boundary data.

To simplify the following discussion, we therefore assume zero external boundary data:  $g_0 = g_\ell = 0$ . Note that condition (22) is sufficient but not necessary for the energy stability of a hyperbolic balance law. Experimental results indicate that the derived scheme is stable for non-zero prescribed forces, moments and velocities. This suggests that an upper-bound exists at least for a suitable class of cases.

We further assume that the external sources are bounded in the sense that  $||q_{\text{ext}}||_{\mathbb{L}^2} < c$  for some  $c \in \mathbb{R}_+$ . By equivalence of norms (using, e.g., Rayleigh's min-max principle from [16]), we obtain:

$$\langle q_{\rm ext}, u \rangle \leq \bar{c} \|u\|_{\Gamma}$$
, for some  $\bar{c} \in \mathbb{R}_+$ .

Inserting this into (20) results in the differential inequality

$$\frac{1}{2} \frac{d}{dt} \|u\|_{\Gamma}^{2} \le \bar{c} \|u\|_{\Gamma} . \tag{23}$$

Integration in time then yields:

$$\|u(\cdot,t)\|_{\Gamma}^2 \le (\|u_0\|_{\Gamma} + \bar{c}t)^2$$
. (24)

To summarize, this provides an upper bound for the energy of the solution of the intrinsic beam equation for zero external boundary data and bounded external forces and moments. In particular, the energy grows at most quadratically in time.

## 3 Discretization

In the following, we discretize the intrinsic beam equations in space using a Discontinuous Galerkin approach based on [6].

## 3.1 A Discontinuous Galerkin Approach for Discretization in Space

We subdivide the domain  $[0, \ell]$  into non-overlapping elements  $\{C_k\}_{k=1,...,N_c}$ :

$$C_{\mathbf{k}} = \left[ x_{\mathbf{k}} - \frac{\Delta x_{\mathbf{k}}}{2} , x_{\mathbf{k}} + \frac{\Delta x_{\mathbf{k}}}{2} \right] .$$

Each element can be mapped linearly onto the reference element  $\mathcal{R} := [-1, 1]$  so that  $x \in C_k$  is mapped to  $\xi(x) = 2/\Delta x_k(x - x_k)$ . By transforming the balance law (16) for the element  $C_k$  to the reference element, we obtain:

$$\frac{\Delta x_{\mathbf{k}}}{2} \left\langle \Gamma u_{t}, \varphi \right\rangle + (\Pi u)^{T} \varphi \Big|_{\xi=-1}^{1} - \left\langle \Pi u, \varphi_{\xi} \right\rangle = \frac{\Delta x_{\mathbf{k}}}{2} \left\langle Q(u), \varphi \right\rangle \ . \tag{25}$$

Here, we substituted the spatial variable x by  $\xi$  using, e.g.,  $u(x,t)|_{C_k} = u(x(\xi),t)|_{\mathcal{R}}$ . Let  $\mathcal{P}_{N_p}(\mathcal{R})$  denote the space of polynomials of degree  $\leq N_p$  on  $\mathcal{R}$ . On each element, the DG discretized approximation of (25) is constructed by approximating the involved functions by polynomials in  $\mathcal{P}_{N_p}(\mathcal{R})$ . As polynomial basis, we use the Legendre polynomials with Gauss-Lobatto quadrature nodes on  $\mathcal{R}$  as interpolation nodes. The interpolation of a function g is denoted by  $I^{N_p}(g)$ . The involved quantities are approximated as follows:

$$\begin{aligned} u|_{C_{k}} &\approx U^{(k)} = I^{N_{p}}(u|_{C_{k}}) ,\\ \Gamma|_{C_{k}} &\approx \Gamma^{(k)} = I^{N_{p}}(\Gamma|_{C_{k}}) ,\\ Q(u)|_{C_{k}} &\approx Q^{(k)} = I^{N_{p}}(Q|_{C_{k}}) . \end{aligned} \tag{26}$$

Thus, the numerical solution is a piecewise polynomial. We use the same polynomial space for the test functions  $\phi \in \mathcal{P}_{N_p}(\mathcal{R})$ . The integrals from the inner product terms are replaced by Gauss-Lobatto quadratures resulting in the discrete inner product denoted by  $\langle \cdot, \cdot \rangle_{N_p}$  and the discrete norm  $\|\cdot\|_{N_p}$ . Similarly, the discrete energy norm  $\|\cdot\|_{N_p,\Gamma}$  is induced by the inner product  $\langle \cdot, \cdot \rangle_{N_p,\Gamma}$ , where  $\langle G, H \rangle_{N_p,\Gamma} = \langle G, \Gamma H \rangle_{N_p}$ . Due to the collocation of quadrature and interpolation nodes, we have for any function g:

$$\langle I^{N_p}(g), \phi \rangle_{N_p} = \langle g, \phi \rangle_{N_p}$$
.

The elements are coupled by replacing the flux,  $\Pi U$ , at the element boundaries by a *numerical flux*  $\mathcal{F}^*$ . Where clear from the context, we omit the element index (k). So Eq. (25) becomes

$$\frac{\Delta x_{\mathbf{k}}}{2} \left\langle \Gamma U_{t}, \phi \right\rangle_{N_{p}} - \left\langle \Pi U, \phi_{\xi} \right\rangle_{N_{p}} - \frac{\Delta x_{\mathbf{k}}}{2} \left\langle Q(U), \phi \right\rangle_{N_{p}} = -\left(\mathcal{F}^{*}\right)^{T} \phi \bigg|_{\xi=-1}^{1} \ . \tag{27}$$

### 3.2 The Numerical Flux

We choose the *Lax-Friedrichs flux*, which is commonly employed for discretizing balance laws, see [6]. In characteristic variables, it is defined as:

$$\bar{\mathscr{F}}^*(W_L, W_R) := \frac{1}{2} \Lambda^*(W_L + W_R) - \frac{\sigma}{2} |\Lambda^*|(W_R - W_L) . \tag{28}$$

Here,  $\sigma \geq 0$  is an upwind parameter,  $(\cdot)^*$  denotes the evaluation of a quantity at an element interface and  $(\cdot)_L$  and  $(\cdot)_R$  denote the left and right limits of the numerical solution at the interface  $(W_L := W^{(k)}(1) \text{ and } W_R = W^{(k+1)}(-1))$ . For the diagonal matrix  $\Lambda$ , the absolute value  $|\Lambda|$  is taken element-wise. For  $\sigma = 0$ , this results in a *central flux*, and for  $\sigma = 1$  in an *upwind flux*.

As we discretize the system in the capacity form, we transform the flux into physical variables using  $W = T^{-1}U$  and multiplying with  $\Gamma^*T^*$  from the left:

$$\mathscr{F}^*(U_L, U_R) := \frac{1}{2} \Pi(U_L + U_R) - \frac{\sigma}{2} (\Gamma|A|)^* (U_R - U_L) . \tag{29}$$

Here,  $|A| := T|\Lambda|T^{-1}$ . Note that the numerical flux is consistent with the capacity form as  $\mathcal{F}^*(U, U) = \Pi U$ .

At the inner element interfaces, we leave the particular choice for  $\sigma$  open. At the physical domain boundaries  $(x = 0, \ell)$ , we prescribe the upwind flux  $\sigma = 1$ . The boundary conditions for the IBVP (14) are then plugged in as *outer* states to compute the boundary flux.

Using a similar notation as for the continuous case, we split the vector  $U = (S^T, Y^T)^T$  into discrete internal forces and moments S and velocities Y. Then, at the boundary x = 0, we choose:

$$U_L = \begin{pmatrix} S_R + (C^{-1/4} \mathcal{M}^{1/2} C^{-1/4})^* (Y_R - y_0) \\ y_0 \end{pmatrix} . \tag{30}$$

At the boundary  $x = \ell$ , we chose:

$$U_R = \begin{pmatrix} s_\ell \\ Y_L - (C^{1/4} \mathcal{M}^{-1/2} C^{1/4})^* (S_L - s_\ell) \end{pmatrix} . \tag{31}$$

These choices are consistent with the original boundary conditions as  $(Y_R - y_0)$  and  $(S_L - s_\ell)$  converge to zero for a converging solution.

## 3.3 Discrete Energy Analysis

We consider the weak form in one element and, analogously to the continuous case, replace  $\phi$  by U. The energy rate in one element is then

$$\frac{\Delta x_{\mathbf{k}}}{4} \frac{\mathbf{d}}{\mathbf{d}t} \left\| U \right\|_{N_p,\Gamma}^2 - \left\langle \Pi U, U_{\xi} \right\rangle_{N_p} - \frac{\Delta x_{\mathbf{k}}}{2} \left\langle Q(U), U \right\rangle_{N_p} = -\left( \mathscr{F}^* \right)^T U \Big|_{\xi=-1}^t . \tag{32}$$

The summation-by-parts property of the Gauss-Lobatto quadrature allows a 'discrete integration by parts' similar to the continuous case in this context, see [6, 17]. So for the volume term, we obtain:

$$-\left\langle \Pi U, U_{\xi} \right\rangle_{N_{p}} = -\frac{1}{2} \left( \Pi U \right)^{T} U \Big|_{\xi = -1}^{1} . \tag{33}$$

Following the same argumentation as for the continuous case in Sect. 2.5, the contribution of the source term vanishes except for the external sources. In total, we obtain

$$\frac{\Delta x_{\mathbf{k}}}{4} \frac{\mathbf{d}}{\mathbf{d}t} \|U\|_{N_{p},\Gamma}^{2} = \frac{\Delta x_{\mathbf{k}}}{2} \langle q_{\mathbf{ext}}, U \rangle_{N_{p}} - \left( U^{T} \mathcal{F}^{*} - \frac{1}{2} U^{T} \Pi U \right) \Big|_{\mathcal{E}=-1}^{1} . \tag{34}$$

This shows the discrete element-wise energy conservation.

Summing up the contributions of all elements, we obtain for the total discrete energy  $\|U\|_{N_{D},\Gamma}^{2}$ :

$$\frac{1}{2} \frac{\mathrm{d}}{\mathrm{d}t} \| U \|_{N_{p},\Gamma}^{2} = \sum_{k=1}^{N_{c}} \frac{\Delta x_{k}}{2} \left\langle q_{\mathrm{ext}}, U^{(k)} \right\rangle_{N_{p}} - \left( \left( U^{(k)} \right)^{T} \mathcal{F}^{*} - \frac{1}{2} \left( U^{(k)} \right)^{T} \Pi U^{(k)} \right) \Big|_{\xi=-1}^{1}.$$

$$(35)$$

We additionally use  $[\cdot]$  to express jumps at element interfaces:

$$[U^{(k)}] = U^{(k)}(1) - U^{(k+1)}(-1) = U_L - U_R$$

and combine all terms on the left and right boundaries with  $b_L$  and  $b_R$ , respectively:

$$\begin{split} b_L &:= - \left( \left( U^{(1)} \right)^T \mathcal{F}^* - \frac{1}{2} \left( U^{(1)} \right)^T \Pi U^{(1)} \right) \bigg|_{\xi = -1} \ , \\ b_R &:= \left. \left( \left( U^{(\mathbf{N_c})} \right)^T \mathcal{F}^* - \frac{1}{2} \left( U^{(\mathbf{N_c})} \right)^T \Pi U^{(\mathbf{N_c})} \right) \right|_{\xi = 1} \ . \end{split}$$

Then, the total discrete energy equation becomes

$$\begin{split} \frac{1}{2} \frac{\mathrm{d}}{\mathrm{d}t} \|U\|_{N_{p},\Gamma}^{2} &= \sum_{\mathbf{k}=1}^{N_{c}} \frac{\Delta x_{\mathbf{k}}}{2} \left\langle q_{\mathrm{ext}}, U^{(\mathbf{k})} \right\rangle_{N_{p}} \\ &- \sum_{\mathbf{k}=1}^{N_{c}-1} \left( \left[ U^{(\mathbf{k})} \right]^{T} \mathcal{F}^{*}(U_{L}, U_{R}) - \frac{1}{2} \left[ \left( U^{(\mathbf{k})} \right)^{T} \Pi U^{(\mathbf{k})} \right] \right) \\ &- b_{L} - b_{R} \; . \end{split} \tag{36}$$

So it contains contributions from external sources, from element interfaces, and from physical boundary conditions, which are considered separately in the following.

## 3.3.1 Contribution of the Interface Terms

Using the definition of the numerical flux and the jump at the interface, the k-th summand of the interface terms in (36) is:

$$\left[U^{(k)}\right]^T \mathcal{F}^*(U_L, U_R) - \frac{1}{2} \left[ \left(U^{(k)}\right)^T \Pi U^{(k)} \right] = \frac{\sigma}{2} \left[U^{(k)}\right]^T (\Gamma |A|)^* \left[U^{(k)}\right] \geq 0,$$

(37)

as  $(\Gamma|A|)^*$  is positive definite [12]. So, we find zero as an upper bound for the corresponding sum in (36) including the negative sign in front. The chosen numerical flux is, therefore, dissipative for  $\sigma > 0$ . For  $\sigma = 0$ , there is no numerical dissipation from the element interfaces.

## 3.3.2 Contribution of the Boundary Terms

Using the definition of the flux, of the boundary terms  $b_L$  and  $b_R$ , and of the outer boundary states  $U_L$  and  $U_R$  for zero boundary data, we obtain:

$$-b_L = -Y_R^T \left( C^{-1/4} \mathcal{M}^{1/2} C^{-1/4} \right)^* Y_R , \qquad -b_R = -S_L^T \left( C^{1/4} \mathcal{M}^{-1/2} C^{1/4} \right)^* S_L .$$

The matrix  $(C^{-1/4}\mathcal{M}^{1/2}C^{-1/4})^*$  is positive definite, so that we have

$$-b_L - b_R \le 0. (38)$$

#### 3.3.3 Contribution of External Sources

For bounded  $q_{\text{ext}}$  (as assumed in Sect. 2.5), we obtain for each element  $C_k$ :

$$\left\langle q_{\mathrm{ext}}, U^{(\mathrm{k})} \right\rangle_{N_p} \le d \left\| U^{(\mathrm{k})} \right\|_{N_p} \text{for some } d \in \mathbb{R}_+ \ .$$

Using the equivalence of the norms  $\|\cdot\|_{N_p}$  and  $\|\cdot\|_{N_p,\Gamma}$  and of *p*-norms for p=1,2 after summing up the contributions of all cells again, we get for some  $\bar{d} \in \mathbb{R}_+$ :

$$\frac{1}{2} \frac{\mathrm{d}}{\mathrm{d}t} \|U\|_{N_p,\Gamma}^2 \le \bar{d} \left( \sum_{k=1}^{N_c} \frac{\Delta x_k}{2} \|U^{(k)}\|_{N_p,\Gamma}^2 \right)^{1/2} = \bar{d} \|U\|_{N_p,\Gamma} . \tag{39}$$

Thus, analogous to the continuous analysis, we obtain:

$$||U(\cdot,t)||_{N_p,\Gamma}^2 \le \left(||U_0||_{N_p,\Gamma} + \bar{d}t\right)^2$$
 (40)

So, the energy of the numerical solution grows at most quadratically in time and the chosen discretization is energy stable.

## 4 Numerical Results

In this section we illustrate the results from the previous sections. We use the numerical simulation framework Trixi.jl [18, 19, 20] to discretize the intrinsic beam equation. For the experiments, we choose constant material parameters:

$$C = \begin{pmatrix} 13 & 6 & 5 & 7 & 8 & 5 \\ 6 & 6 & 4 & 3 & 5 & 4 \\ 5 & 4 & 5 & 3 & 5 & 4 \\ 7 & 3 & 3 & 7 & 4 & 3 \\ 8 & 5 & 5 & 4 & 9 & 5 \\ 5 & 4 & 4 & 3 & 5 & 5 \end{pmatrix}, \qquad \mathcal{M} = \begin{pmatrix} 12 & 4 & 5 & 5 & 10 & 3 \\ 4 & 4 & 2 & 3 & 4 & 1 \\ 5 & 2 & 8 & 6 & 6 & 2 \\ 5 & 3 & 6 & 8 & 7 & 3 \\ 10 & 4 & 6 & 7 & 13 & 5 \\ 3 & 1 & 2 & 3 & 5 & 4 \end{pmatrix}. \tag{41}$$

These do not describe any realistic material properties as the goal is only to illustrate the numerical behavior. For the discretization in time, we use the *Low-Storage-Five-Stage Fourth-Order Explicit Runge-Kutta Method* (LSERK) from [21].

## 4.1 Convergence Tests

To analyse the convergence of the numerical solution, we use manufactured solutions as in [22]: We use  $u = \bar{u} := (\bar{u}_m)_{m=1,\dots,12}$  with

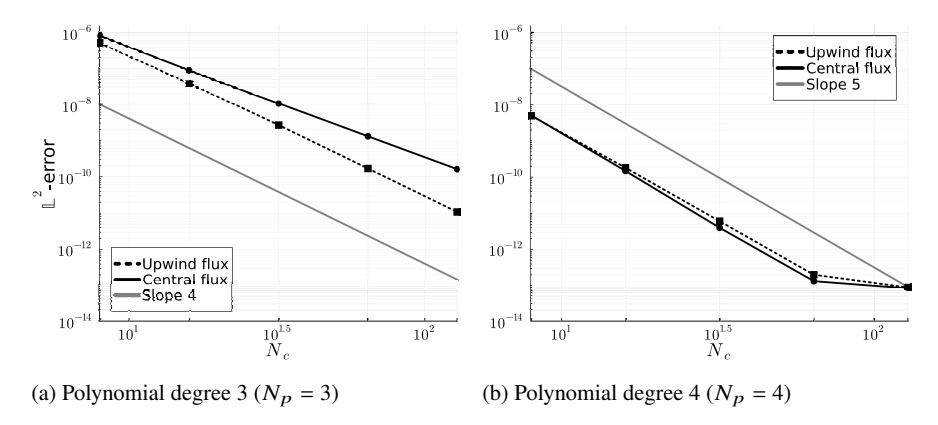


Fig. 1: Plot of the average  $\mathbb{L}^2$ -error for different number of elements and  $N_p = 3,4$ 

$$\bar{u}_m(x,t) := \begin{cases} t \sin(\pi/2 (1-x)) & m = 1, \dots, 6 \\ t \sin(\pi/2 x) & m = 7, \dots, 12 \end{cases}$$
 (42)

We insert this function into the homogeneous part of the capacity form, i.e., without the source term. This results in a residual  $r = \Gamma \bar{u}_t + \Pi \bar{u}_x$  and can be interpreted as:

$$\Gamma \bar{u}_t + \Pi \bar{u}_x = Q(\bar{u}) + r - Q(\bar{u}) . \tag{43}$$

So  $\bar{u}$  satisfies the original problem with the additional source term  $r - Q(\bar{u})$ . While the original source term in Trixi.jl is evaluated at the numerical solution, we evaluate the Q in the additional source term at the exact  $\bar{u}$ . As the numerical solution converges to the exact solution, the source terms cancel each other out. We further set the external forces and moments and the initial curvature to zero, and choose the length  $\ell = 1$  and the end time T = 1.

In Fig. 1, we show resulting errors for different spatial resolutions, polynomial degrees 3 and 4, and upwind, respectively central flux. For  $N_p = 3$ , we observe an optimal convergence order of  $(N_p + 1)$  with the upwind flux. For the central flux, we observe a convergence order of  $N_p$ . This is the expected behavior for the scheme, see [5]. For  $N_p = 4$ , both solutions converge with the optimal convergence order of  $(N_p + 1)$  and reach the machine accuracy for the highest spatial resolutions.

## 4.2 Energy Simulation

We showed that the discrete energy grows at most quadratically in time for zero boundary condition and bounded external forces and moments. In case of zero external forces, the discrete energy is non-increasing which we illustrate in another numerical simulation.

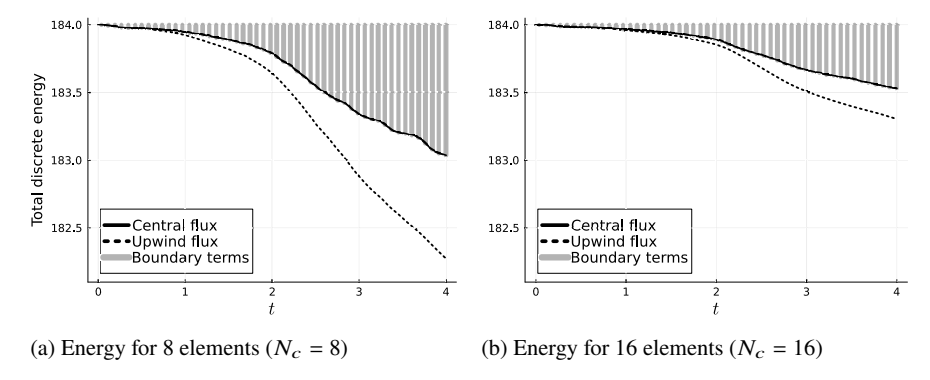


Fig. 2: Total discrete energy of the solution

We use a similar setup as before but simulate the beam until T=4. As initial condition, we choose  $u_0(x)=\bar{u}(x,1)$ . The total discrete energy of the numerical solution is depicted in Fig. 2.

In absence of external forces and moments, the energy of the exact solution is constant. We observe that the discrete energy of the numerical solution decreases. As expected, the simulations using the upwind flux show a higher dissipation than the ones using the central flux. The dissipation for the cases using the central flux results from the physical boundary conditions where we always use the upwind flux. In a post-processing step, we evaluated the accumulated energy dissipation resulting from fluxes at the boundaries which is shown for discrete points in time in Fig. 2 We see that the amount of dissipation from the boundary approximately matches the amount of total dissipation for the central flux. Due to the numerical error of the discretization in time, there is no exact match between the accumulated energy dissipation terms at the boundary and the dissipated total discrete energy. The maximal difference is about  $1.33 \times 10^{-3}$  for 8 elements and  $3.02 \times 10^{-4}$  for 16 elements which is within the expected tolerance.

When increasing the spatial resolution (8 to 16 elements), we obtain less dissipation as the numerical solution converges to the exact solution.

## 5 Conclusion and Outlook

We showed that the energy stability of the continuous intrinsic beam equations transfers to the discrete context for a Discontinuous Galerkin (DG) discretization of a clamped-free beam with appropriate choices of numerical fluxes and boundary conditions. We illustrated our results using numerical simulations with the DG framework Trixi.jl.

For future work, we will investigate the discretization of the intrinsic beam equations with additional damping terms such as, e.g., the intrinsic beam model with

Kelvin-Voigt damping introduced in [23]. Even though at first sight, the damping seems to introduce only minor changes in the equations, it introduces additional derivatives which need to be handled appropriately in the discretization and the energy stability analysis. The damping model is crucial to tackle real-world problems from rotorcraft design.

## References

- 1. D.H. Hodges, AIAA Journal 41(6), 1131 (2003). DOI 10.2514/2.2054
- M.R. Amoozgar, H. Shahverdi, A.S. Nobari, AIAA Journal 55(7), 2450 (2017). DOI 10.2514/ 1.j055079
- Z. Sotoudeh, D.H. Hodges, Journal of the American Helicopter Society 58(3), 1 (2013). DOI 10.4050/jahs.58.032004
- C. Rodriguez, G. Leugering, SIAM Journal on Control and Optimization 58(6), 3533 (2020). DOI 10.1137/20m1340010
- J.S. Hesthaven, T. Warburton, Nodal Discontinuous Galerkin Methods (Springer New York, 2008). DOI 10.1007/978-0-387-72067-8
- D.A. Kopriva, G.J. Gassner, SIAM Journal on Scientific Computing 36(4), A2076 (2014). DOI 10.1137/130928650
- D.A. Kopriva, G.J. Gassner, Journal of Scientific Computing 89(1) (2021). DOI 10.1007/ s10915-021-01618-5
- Y. Xing, C.W. Shu, Journal of Computational Physics 214(2), 567 (2006). DOI 10.1016/j.jcp. 2005.10.005
- C. Rodriguez, Control and stabilization of geometrically exact beams. Ph.D. thesis, Friedrich-Alexander-Universität Erlangen-Nürnberg (2022). DOI 10.48550/ARXIV.2202.07531
- 10. M.J. Patil, D.H. Hodges, Journal of Aircraft 43(6), 1790 (2006). DOI 10.2514/1.17640
- A. Wynn, Y. Wang, R. Palacios, P.J. Goulart, Journal of Sound and Vibration 332(21), 5543 (2013). DOI 10.1016/j.jsv.2013.05.021
- 12. C. Bleffert, An energy stable discontinuous galerkin discretization approach for the geometrically exact intrinsic beam model. Master's thesis, Universität zu Köln (2022)
- Z. Sotoudeh, D.H. Hodges, Journal of Applied Mechanics 78(3) (2011). DOI 10.1115/1. 4003239
- J. Nordström, M. Wahlsten, Journal of Computational Physics 282, 1 (2015). DOI 10.1016/j. jcp.2014.10.061
- J. Nordström, Journal of Scientific Computing 71(1), 365 (2016). DOI 10.1007/ s10915-016-0303-9
- R.A. Horn, C.R. Johnson, *Matrix Analysis* (Cambridge University Press, 1985). DOI https://doi.org/10.1017/CBO9780511810817
- D.A. Kopriva, G.J. Gassner, Journal of Scientific Computing 44(2), 136 (2010). DOI 10.1007/ s10915-010-9372-3
- H. Ranocha, M. Schlottke-Lakemper, A.R. Winters, E. Faulhaber, J. Chan, G.J. Gassner, Proceedings of the JuliaCon Conferences 1(1), 77 (2022). DOI 10.21105/icon.00077
- M. Schlottke-Lakemper, A.R. Winters, H. Ranocha, G.J. Gassner, Journal of Computational Physics 442, 110467 (2021). DOI 10.1016/j.jcp.2021.110467
- 20. M. Schlottke-Lakemper, G.J. Gassner, H. Ranocha, A.R. Winters, J. Chan. Trixi.jl: Adaptive high-order numerical simulations of hyperbolic PDEs in Julia. https://github.com/trixi-framework/Trixi.jl (2021). DOI 10.5281/zenodo.3996439
- M.H. Carpenter, C.A. Kennedy, NASA Report TM 109112, NASA Langley Research Center (1994)
- 22. P.J. Roache, Journal of Fluids Engineering **124**(1), 4 (2001). DOI 10.1115/1.1436090
- 23. M. Artola, A. Wynn, R. Palacios, AIAA Journal 59(1), 356 (2021). DOI 10.2514/1.j059767